Human adherent cortical organoids in a multiwell format

Mark van der Kroeg[1], Sakshi Bansal[1], Maurits Unkel[1], Hilde Smeenk[1,] Steven A. Kushner[1,2,3#*], Femke M.S. de Vrij[1,4#*]

[1]Department of Psychiatry, Erasmus MC University Medical Center, Rotterdam, The Netherlands.

[2]Department of Psychiatry, Columbia University Irving Medical Center, New York, NY, USA

[3]Stavros Niarchos Foundation (SNF) Center for Precision Psychiatry & Mental Health, Columbia University, New York, NY, USA

[4]ENCORE Expertise Center for Neurodevelopmental Disorders, Erasmus MC, Rotterdam, The Netherlands

[#]These authors contributed equally

Contact information: *Correspondence: sk2602@cumc.columbia.edu, f.devrij@erasmusmc.nl.

Summary

In the growing diversity of human iPSC-derived models of brain development, we present here a novel method that exhibits 3D cortical layer formation in a highly reproducible topography of minimal dimensions. The resulting adherent cortical organoids develop by self-organization after seeding frontal cortex patterned iPSC-derived neural progenitor cells in 384-well plates during eight weeks of differentiation. The organoids have stereotypical dimensions of 3 x 3 x 0.2 mm, contain multiple neuronal subtypes, astrocytes and oligodendrocyte lineage cells, and are amenable to extended culture for at least 10 months. Longitudinal imaging revealed morphologically mature dendritic spines, axonal myelination, and robust neuronal activity. Moreover, adherent cortical organoids compare favorably to existing brain organoid models on the basis of robust reproducibility in obtaining topographically-standardized singular radial cortical structures and circumvent the internal necrosis that is common in free-floating cortical organoids. The adherent human cortical organoid platform holds considerable potential for high-throughput drug discovery applications, neurotoxicological screening, and mechanistic pathophysiological studies of brain disorders.

Introduction

Using human embryonic or induced pluripotent stem cell (hiPSC) derived models to investigate the developing brain in health and disease has yielded considerable success (Marton and Pașca, 2020). The approaches have been varied, including single cell hiPSC-derived models grown in a monolayer (Sarkar et al., 2018; Zhang et al., 2013), multiple neural cell types in 2D neural networks (Astick and Vanderhaeghen, 2018; Bardy et al., 2015; Gunhanlar et al., 2018; Shi et al., 2012), 3D free-floating regionalized neural organoids (Paşca et al., 2015; Qian et al., 2016a; Xiang et al., 2019; Zhang et al., 2023), and hiPSC-derived free-floating unguided neural organoids (Gomes et al., 2020; Lancaster et al., 2013; Pașca et al., 2022; Pellegrini et al., 2020; Renner et al., 2017; Sawada et al., 2020). Among the consistent findings across models is that increasing cellular and topographical complexity has appeared to come at the cost of increased variability (Eichmüller and Knoblich, 2022; Kelava and Lancaster, 2016). Therefore, a major current technical challenge is to identify hiPSC-derived models that recapitulate higher-order neural complexity with reduced heterogeneity.

Existing 3D models suffer from considerable variability due to the complex and heterogeneous nature of the free-floating structures (Cederquist et al., 2019; Lancaster et al., 2013, 2017; Paşca et al., 2015; Renner et al., 2017; Velasco et al., 2019; Yoon et al., 2019). A further challenge, in particular with free-floating organoids, is the necrotic core that emerges when tissue volumes exceed the limits of oxygen and nutrient diffusion beyond a radius of ~300-400μm (Lancaster et al., 2017; Qian et al., 2016b). Although recent progress has been made with slicing organoids prior to the emergence of necrosis followed by organotypic air-liquid interface culture (Giandomenico et al., 2019; Qian et al., 2020), even sliced organoids have to be repeatedly re-cut to prevent necrosis (Qian et al., 2020),

which is both laborious and risks introducing another potential source of variability. The generation of vascularized organoids would be the ultimate solution to reduce the necrotic core and the inherent stress that is observed in cortical organoids (Bhaduri et al., 2020; Fan et al., 2022). It will be beneficial to have increased diffusion through microfluidics or vascularization (current efforts summarized in Matsui et al., 2021) and further study the mutually beneficial interaction of neural cells and vascular cells (Crouch et al., 2022; Mansour et al., 2018; Wang et al., 2023).

Here we propose a simplified approach to generating long-term hiPSC-derived adherent cortical organoids with reproducible dimensions and the potential for high-throughput screening in a 384-well format. The resulting adherent cortical organoids can be maintained in long-term culture and contain neurons with dendritic spines and robust activity, as well as several classes of glial cells including oligodendrocyte precursor cells, myelinating oligodendrocytes, and morphologically distinct sub-types of astrocytes.

Results

Self-organized topography of iPSC-derived adherent cortical organoids

Adherent cortical organoids reproducibly self-organized into layered radial structures in 384-wells plates within 8 weeks of seeding with hiPSC-derived forebrain-patterned neural progenitor cells (NPCs). Three different hiPSC source cell lines were used in this study, including commercially available NPCs, and NPCs generated using a modified version of our previously described protocol (Gunhanlar et al., 2018) (**Figure 1A**). NPCs were capable of neural rosette formation and expressed SOX2, Nestin, and the frontal cortical NPC-marker FOXG1 (**Figure 1B, C, D, Figure S1A).** The initial 4 weeks after seeding the NPCs in Neural Differentiation Medium (ND) were characterized by proliferative expansion of NPCs and the emergence of early neural differentiation markers (**Figure 1E, Figure S2**). Between 4- and 8-weeks post-seeding, neurons and glial cells emerged with a consistent spatial organization (**Figure 1E, F, Figure S1B, Figure S2**), in which the central region was densely packed with cell bodies while the periphery contained circumferentially and radially organized processes originating from cells in the centre. Typically, cortical organoids defined as a single radial structure per well were observed in ~80% of the wells seeded with NPCs after 60 days of differentiation. The structural integrity of single structure organoids remained quite stable and slowly diminished over time to about 50% of intact single structure organoids after 1 year in culture (**Figure S1D**). Organoid structure formation was highly dependent on the proliferation rate of NPCs, that can differ substantially between differentiation batches and hiPSC clones. Plotting the interaction between proliferation and the amount of NPCs required to be seeded for the successful generation of adherent cortical organoids, showed a significant correlation (r^2=0.67) that can be used as a guideline for testing a range of NPC densities (**Figure S1C**). For each NPC line an optimal seeding density was estimated based on

the proliferation rate of that NPC line. Multiple densities were seeded around the estimated optimal density and after 6 weeks it was visually determined which NPC density enabled adherent cortical organoid generation. Typically, too sparse seeding density generated neural networks lacking structure, while excessive densities resulted in overgrowth, leading to reduced structural organisation and compromised long-term survival.

Cell type distribution and layer formation

The spatial organisation that evolved over the first 8 weeks after seeding was paralleled by a shift in cell type distribution. Tau+/MAP2- axons exhibited long extensions in a circular pattern, while MAP2+ dendrites exhibited orthogonally-oriented radial outgrowth (**Figure 2A, Figure S3**).

Overall, a reduction in progenitor markers (SOX2 day 14: 58.4%, day 56: 18.8% P = <0.001, PAX6 day 14: 34.5%, day 56: 8.0% P = 0.20) and a significant increase in neuronal cortical layer markers (CTIP2 day 14: 0.5%, day 56: 14.0% P = <0.001, CUX1 day 14: 1.3%, day 56: 24.4% P = <0.001) were observed (**Figure S2**). Cortical layer markers exhibited an inside-out pattern of development in which expression of the deep layer excitatory neuronal marker CTIP2 emerged before the upper layer marker CUX1 (**Figure S2**, **Figure 2C**). After 6-8 weeks following seeding, a self-organised rudimentary segregation of deep- and upper layer neurons emerged as shown by a clear macroscopic separation of deep- and upper layer neurons, although some neurons were spatially intermixed and some neurons were double-positive for CTIP2 and CUX1. Segregation was also observed between CUX1 and CUX2 positive cells as CUX2 is typically expressed over a wider range of upper cortical layers than CUX1 and also marks intermediate progenitors (Molyneaux et al., 2007) (**Figure**

2C, Figure S4). Analogous to the broad distribution of cortical cell subclasses, the majority of the neurons were glutamatergic, while GAD67+ interneurons were also present (**Figure 2D**), constituting ~10% of the NeuN-positive neuronal population consistently for all three source hiPSC lines (**Figure S5**).

Adherent cortical organoids contain multiple glial cell types

Within 8 weeks of seeding, a population of GFAP+/S100β+ astrocytes emerged. Many astrocytes had their soma located in the central region with process outgrowth radially (**Figure 2E, Figure S6**), while other astrocytes exhibited subtype-specific morphologies including fibrous astrocytes (**Figure 2F**), protoplasmic-like astrocytes (**Figure 2G**) and interlaminar astrocytes (**Figure 2H**). GFAP/PAX6 double-positive radial glia were present at the outskirts of the densely populated centre of the organoid with processes growing radially outwards (**Figure 2I**). Similar to free-floating organoids, adherent cortical organoids survived for longer periods compared to monolayer neural cultures grown on larger surfaces. The longevity allows for the development of cell types not usually seen in a monolayer culture that can typically be cultured up to a maximum of 2 to 3 months. By 6 weeks after seeding NPCs we observed the emergence of oligodendrocyte precursor cells (OPC), as shown by the expression of NG2 (**Figure 3A**). NG2+ cells remained present until at least 4 months **(Figure 3B/C)**. Staining for Myelin Basic Protein (MBP) revealed the emergence of MBP+ oligodendrocytes around 4 months after NPC seeding when the organoids were continuously grown in the presence of T3 (2ng/ml) **(Figure 3D)**. At 5 months, the oligodendrocytes showed increasingly mature morphologies (**Figure 3E-I**) and exhibited MBP co-localization along NF200+ axons (**Figure 3F/I**).

Adherent cortical organoids show synaptic connectivity and functional activity

Neurons within adherent cortical organoids exhibited clear evidence of synaptogenesis (**Figure 4A-D**). Sparse labelling of excitatory neurons with AAV9.CamKII.eGFP revealed the presence of Synapsin-positive (Syn+) mushroom-shaped dendritic spines (**Figure 4E**). To assess the functional activity of the cortical organoids, we used the genetically-encoded calcium indicator GCaMP6s under the control of the human Synapsin promoter (**Figure 4F**), allowing cell-type specific quantification of neuronal activity. Calcium imaging revealed robust synchronous network-level bursting (NB) (1.4 ± 0.07 NB/min) in which the vast majority of recorded neurons participated. In addition, substantial desynchronized activity was also observed (3.9 ± 0.5 events/min) during time periods outside of network-level bursting (**Figure 4G-J, Figure 4 – Video 1**).

Discussion

The study of early human brain development and related diseases has long been hampered by the inherent complexity of the human brain and the inaccessibility of living brain tissue at cellular resolution. Technological advances in induced pluripotent stem cell technology have now facilitated the opportunity to obtain living human neurons derived from specific individuals.

We describe here a platform to model early human frontal cortical development with high reproducibility and simplified organization. While 3D floating organoids, or sliced organoids, nicely recapitulate layered cortex formation, they are subject to variation in the relative contribution of cortical tissue within the organoid, forming multiple cortical patches along the edges and complicating structured analysis (Eichmüller and Knoblich, 2022; Giandomenico et al., 2019; Quadrato et al., 2017). Moreover, 3D floating organoids suffer

from necrosis in the core of the organoid due to lack of oxygen and nutrient diffusion. Recently, other protocols have been published starting from rosette formation with a focus on very early development and leading to single structure free floating cortical organoids(Pagliaro et al., 2023; Tidball et al., 2023). Our platform predefines a rosette-forming iPSC-derived cortical NPC population that self-organizes into adherent singular radial structures in a standard 384-well format. Other examples have highlighted the benefits of a multi-well format or systematic individual structure formation (Knight et al., 2018; Medda et al., 2016). Our platform now integrates these features to yield individual adherent layered cortical structures with robust functional synaptic connectivity and neuronal activity and including advanced glial cell types such as myelinating oligodendrocytes and subclasses of astrocytes. The small reproducible format of the organoids in a 384-well format has the distinct advantage of being able to image entire organoids without slicing or clearing and to perform spatiotemporal functional analysis by fluorescence-based calcium imaging. We confirmed the self-organizing potential and reproducibility of adherent cortical organoids across multiple hiPSC lines and using different sources of NPCs, controlling the seeding density for the proliferation rate of the specific NPC batch. Seeding NPCs with frontal cortical identity in the defined geometry of a 384-well plate enabled the development of long-term functional neural networks in a complex radial structure resembling early human cortical development. Future studies aimed at single cell gene expression analysis and advanced image-based analysis solutions in this platform will be interesting in the context of the increasing knowledge on single cell topographical, typological and temporal hierarchies in the developing human cortex (Bhaduri et al., 2021; Nowakowski et al., 2017, 2016; Uzquiano et al., 2022).

These functional adherent cortical organoids in a multi-well format should be amenable to high-throughput screening applications, mechanistic pathophysiological studies of neurodevelopmental and neuropsychiatric disorders, and pharmacological and phenotypic screening of disease phenotypes during early cortical development. Moreover, toxicological studies for novel therapeutic compounds also show an increasing need for testing specific effects in human neuronal models, whereas studies using rodent models have often shown poor predictive power for drug safety and efficacy in human central nervous system disorders (van Esbroeck et al., 2017).

Adherent cortical organoids also have some limitations, as the current iteration of adherent cortical organoids exhibits limited cortical layering and regional specification, that seem to be more advanced in floating whole brain organoids. However, these drawbacks are offset by significantly enhanced ease and higher-throughput possibilities of downstream analysis applications.

Taken together, we present a novel platform for cellular-level human brain modeling using adherent cortical organoids that exhibit high reproducibility and robust neuronal activity. The ability to reliably generate human cortical organoids in multi-well plates combined with neural network functionality offers a unique potential for brain disease modeling and therapeutic screening applications.

Materials and Methods

Generation of Neural Progenitor Cells

NPCs from 3 different source hiPSC lines were used. NPC-line 1: in house generated NPCs from human iPSC line WTC11 (Provided by Bruce R. Conklin, The Gladstone Institutes and UCSF, #GM25256, RRID:CVCL_Y803, Miyaoka et al.,2014). NPC-line 2: commercially available hNPCs from Axol Biosciences (ax0015). NPC-line 3: NPCs derived using the protocol of Shi et al., (Shi et al., 2012) from hiPSC line IPSC0028 (Sigma-Aldrich, RRID:CVCL_EE38). Line 1 NPCs were generated as previously described from hiPSCs grown on a mouse embryonic fibroblast (MEF) feeder layer (Gunhanlar et al., 2018). After passage 3, NPC cultures were purified using fluorescence-activated cell sorting (FACS). NPCs were detached from the culture plate using Accutase (Stem Cell Technologies) and $CD184^{+}/CD44^{-}/CD271^{-}/CD24^{+}$ cells (Yuan et al., 2011) were collected on a FACSAria III Cell Sorter (BD Bioscience) and expanded in NPC medium consisting of: DMEM/F12, 1% N2 supplement, 2% B27-RA supplement (Thermo Fisher Scientific), 1 µg/ml laminin (L2020, Sigma-Aldrich), 20 ng/ml basic fibroblast growth factor (Merck-Millipore, Darmstadt, Germany) and 1% penicillin/streptomycin (Thermo Fisher Scientific). NPCs were differentiated to adherent cortical organoids between passage 3 and 7 after sorting.

Neural differentiation

384-well plates (M1937-32EA. Life Technologies) were coated with 50 µg/ml laminin in dH_20 (Sigma, L2020) for 30 minutes at 37°C. The NPCs in NPC medium were dissociated with Accutase (Stem Cell Technologies), live cells were counted with Trypan Blue (Stem Cell Technologies) in a Burker counting chamber. The NPCs were seeded in the wells of a 384-well plate at defined densities for each cell line. Specifically, the optimal seeding density was

determined by visual inspection of the organoids between 28 to 42 days after seeding a range of cell densities in the 384-well plate wells. NPCs were seeded and differentiated in Neural Differentiation Medium: Neurobasal medium (Thermo Fisher Scientific), 1% N2 supplement (Thermo Fisher Scientific), 2% B27-RA supplement (Thermo Fisher Scientific), 1% minimum essential medium/non-essential amino acid (Stem Cell Technologies), 20 ng/ml brain-derived neurotrophic factor (ProSpec Bio), 20 ng/ml glial cell-derived neurotrophic factor (ProSpec Bio), 1 µM dibutyryl cyclic adenosine monophosphate (Sigma-Aldrich), 200 µM ascorbic acid (Sigma-Aldrich), 2 µg/ml laminin (Sigma-Aldrich) and 1% penicillin/streptomycin (Thermo Fisher Scientific). For oligodendrocyte maturation the cells were grown in the presence of 2 ng/ml T3 (Sigma-Aldrich). Cells were refreshed every 2-3 days.

Immunocytochemistry

For live-dead staining, living cultures were incubated with LIVE/DEAD™ Viability/Cytotoxicity Kit according to manufacturer's instructions (Thermo Fisher Scientific). For immunocytochemistry adherent cortical organoids were fixed for 20-30 minutes using 4% formaldehyde in phosphate-buffered saline (PBS), washed with PBS and blocked for 1 hour by pre-incubation in staining buffer containing 0.05 M Tris, 0.9% NaCl, 0.25% gelatin and 0.5% Triton-X-100 (pH 7.4). Primary antibodies were incubated for 48-72h at 4 °C in staining buffer, washed with PBS and incubated with the secondary antibodies in staining buffer for 2h at room temperature. The cultures were embedded in Mowiol 4-88 (Sigma-Aldrich), after which confocal imaging was performed with a Zeiss LSM700 and Zeiss LSM800 confocal microscope using ZEN software (Zeiss, Oberkochen, Germany). The following primary antibodies were used: SOX2 (Merck-Millipore AB5603, 1:200); Nestin (Merck-Millipore

MAB5326, 1:200); MAP2 (Synaptic Systems 188004, 1:100); NeuN (Merck ABN78, 1:200); GFAP (Merck-Millipore AB5804, 1:300); FOXG1 (Abcam AB18259, 1:200); CUX1 (Abcam AB54583, 1:200); CTIP2 (Abcam AB18465, 1:100); Synapsin 1/2 (Synaptic Systems 106003, 1:200); and PSD95 (Thermo Fisher Scientific MA1-046, 1:100); Tau (Cell Signaling Technology 4019, 1:200); S100ß (Sigma-Aldrich S2532, 1:200); Pax6 (Santa Cruz sc-81649, 1:100); NG2 (Gift from W. Stallcup Lab, 1:100); NF200 (Sigma-Aldrich 083M4833 1:200); MBP (Abcam AB7349, 1:100); GFP (Abcam ab13970, 1:100); GAD67 (Merck-Millipore MAB5406, 1:100) DAPI (Thermo Fisher Scientific D1306). The following secondary antibodies were used 1:200: Alexa-488, Alexa-555, Alexa-647 (Jackson ImmunoResearch, West Grove, PA, USA).

Sparse labelling of excitatory neurons

pENN.AAV9.CamKII.4.eGFP.WPRE.rBG (Addgene viral prep # 105541-AAV9) was added to the cortical organoids at day 278 ($1.68x10^8$ GC/well). The transduced cortical organoids were fixed and stained at day 310.

Calcium imaging

For calcium imaging the genetically encoded calcium indicator AAV1.Syn.GCaMP6s.WPRE.SV40 (Penn Vector Core, 100843-AAV1) was added to the organoids at day 42 of differentiation ($1.5x10^8$ GC/well). Recordings were performed at day 60 on a Zeiss LSM800 confocal microscope using ZEN software (Zeiss, Oberkochen, Germany). The recordings were made with a 20x/0.8NA Ph2 Plan-Apochromat objective, with a field of view of 150 × 100 µm and a pixel size of 0,3 µm. The acquisition rates of the recordings were between 4-5 f.p.s. 24 hours before the recordings, the medium was switched to BrainPhys Neural Differentiation Medium. BrainPhys Neuronal Media (Stem Cell

Technologies), 1% N2 supplement (Thermo Fisher Scientific), 2% B27-RA supplement (Thermo Fisher Scientific), 1% minimum essential medium/non-essential amino acid (Stem Cell Technologies), 1% penicillin/streptomycin (Thermo Fisher Scientific), 20 ng/ml brain-derived neurotrophic factor (ProSpec Bio), 20 ng/ml glial cell-derived neurotrophic factor (ProSpec Bio), 1 µM dibutyryl cyclic adenosine monophosphate (Sigma-Aldrich), 200 µM ascorbic acid (Sigma-Aldrich) and 2 µg/ml laminin (Sigma-Aldrich). The calcium imaging recordings were processed using CNMF-E (Pnevmatikakis et al., 2016). Calcium traces were then analysed using a custom script for event and network burst detection using an algorithm written in Python (v3.8.2) (code accessibility can be requested via Github).

Cyquant Proliferation Assay

CyQUANT™ Direct Cell Proliferation Assay, C35011 (Thermo Fisher Scientific) was used according to manufacturer specifications. For each time point and each of the 3 NPC lines 10-12 wells of a 96-well plate were seeded with NPCs (2500 NPCs per well). In addition, NPC lines generated from 2 different clones from IPS line MH0159020 (Rutgers University Cell and DNA Repository) were added to increase the dynamic range of the proliferation curve. At 24h and 96h NPCs were frozen at -80°C. All NPC lines and timepoints were thawed, lysed and measured together. Doubling time was calculated between 24h and 96h. None of the wells was confluent at 96h.

Statistical analysis

All data represent mean ± SEM. When comparing developmental markers in Figure S2 we used one-way ANOVA followed by Tukey- Kramer's multiple correction test. n=3-6 images taken over two wells, for each time point.

Acknowledgements

This work was supported by the Netherlands Organ-on-Chip Initiative, an NWO Gravitation project funded by the Ministry of Education, Culture and Science of the government of the Netherlands (024.003.001) to SAK, Hersenstichting Fellowship (F2012(1)-39) to FMSdV, an Erasmus MC Human Disease Model Award to FMSdV and a Dutch ZonMw MKMD Create2Solve grant (114025201) to SAK and FMSdV.

Author contributions

MvdK, SB and HS performed experiments, MU developed calcium imaging analysis algorithms, FdV and SAK supervised the work, MvdK, FdV and SAK wrote the paper.

Declaration of interests

The authors declare no competing interests.

References

Astick M, Vanderhaeghen P. 2018. From Human Pluripotent Stem Cells to Cortical Circuits. *Curr Top Dev Biol* **129**:67–98. doi:10.1016/bs.ctdb.2018.02.011

Bardy C, van den Hurk M, Eames T, Marchand C, Hernandez R V, Kellogg M, Gorris M, Galet B, Palomares V, Brown J, Bang AG, Mertens J, Böhnke L, Boyer L, Simon S, Gage FH. 2015. Neuronal medium that supports basic synaptic functions and activity of human

neurons in vitro. *Proc Natl Acad Sci U S A* **112**. doi:10.1073/pnas.1504393112

Bhaduri A, Andrews MG, Mancia Leon W, Jung DD, Shin D, Allen D, Jung DD, Schmunk G, Haeussler M, Salma J, Pollen AA, Nowakowski TJ, Kriegstein AR. 2020. Cell stress in cortical organoids impairs molecular subtype specification. *Nature* 1–7. doi:10.1038/s41586-020-1962-0

Bhaduri A, Sandoval-Espinosa C, Otero-Garcia M, Oh I, Yin R, Eze UC, Nowakowski TJ, Kriegstein AR. 2021. An atlas of cortical arealization identifies dynamic molecular signatures. *Nature* **598**:200–204. doi:10.1038/s41586-021-03910-8

Cederquist GY, Asciolla JJ, Tchieu J, Walsh RM, Cornacchia D, Resh MD, Studer L. 2019. Specification of positional identity in forebrain organoids. *Nat Biotechnol* **37**:436–444. doi:10.1038/s41587-019-0085-3

Crouch EE, Bhaduri A, Andrews MG, Cebrian-Silla A, Diafos LN, Birrueta JO, Wedderburn-Pugh K, Valenzuela EJ, Bennett NK, Eze UC, Sandoval-Espinosa C, Chen J, Mora C, Ross JM, Howard CE, Gonzalez-Granero S, Lozano JF, Vento M, Haeussler M, Paredes MF, Nakamura K, Garcia-Verdugo JM, Alvarez-Buylla A, Kriegstein AR, Huang EJ. 2022. Ensembles of endothelial and mural cells promote angiogenesis in prenatal human brain. *Cell* **185**:3753-3769.e18. doi:10.1016/j.cell.2022.09.004

Eichmüller OL, Knoblich JA. 2022. Human cerebral organoids — a new tool for clinical neurology research. *Nat Rev Neurol* **18**:661–680. doi:10.1038/s41582-022-00723-9

Fan W, Christian KM, Song H, Ming G li. 2022. Applications of Brain Organoids for Infectious Diseases. *J Mol Biol* **434**:167243. doi:10.1016/j.jmb.2021.167243

Giandomenico SL, Mierau SB, Gibbons GM, Wenger LMD, Masullo L, Sit T, Sutcliffe M, Boulanger J, Tripodi M, Derivery E, Paulsen O, Lakatos A, Lancaster MA. 2019. Cerebral organoids at the air–liquid interface generate diverse nerve tracts with functional

output. *Nat Neurosci* **22**:669–679. doi:10.1038/s41593-019-0350-2

Gomes AR, Fernandes TG, Vaz SH, Silva TP, Bekman EP, Xapelli S, Duarte S, Ghazvini M, Gribnau J, Muotri AR, Trujillo CA, Sebastião AM, Cabral JMS, Diogo MM. 2020. Modeling Rett Syndrome With Human Patient-Specific Forebrain Organoids. *Front Cell Dev Biol* **8**:1–18. doi:10.3389/fcell.2020.610427

Gunhanlar N, Shpak G, van der Kroeg M, Gouty-Colomer LA, Munshi ST, Lendemeijer B, Ghazvini M, Dupont C, Hoogendijk WJG, Gribnau J, de Vrij FMS, Kushner SA. 2018. A simplified protocol for differentiation of electrophysiologically mature neuronal networks from human induced pluripotent stem cells. *Mol Psychiatry* **23**:1336–1344. doi:10.1038/mp.2017.56

Kelava I, Lancaster MAA. 2016. Stem Cell Models of Human Brain Development. *Cell Stem Cell* **18**:736–748. doi:10.1016/j.stem.2016.05.022

Knight GT, Lundin BF, Iyer N, Ashton LMT, Sethares WA, Willett RM, Ashton RS. 2018. Engineering induction of singular neural rosette emergence within hPSC-derived tissues. *Elife* **7**. doi:10.7554/eLife.37549

Lancaster M a, Renner M, Martin C-A, Wenzel D, Bicknell LS, Hurles ME, Homfray T, Penninger JM, Jackson AP, Knoblich JA. 2013. Cerebral organoids model human brain development and microcephaly. *Nature* **501**:373–379. doi:10.1038/nature12517

Lancaster MA, Corsini NS, Wolfinger S, Gustafson EH, Phillips AW, Burkard TR, Otani T, Livesey FJ, Knoblich JA. 2017. Guided self-organization and cortical plate formation in human brain organoids. *Nat Biotechnol* **35**:659–666. doi:10.1038/nbt.3906

Mansour AA, Gonçalves JT, Bloyd CW, Li H, Fernandes S, Quang D, Johnston S, Parylak SL, Jin X, Gage FH. 2018. An in vivo model of functional and vascularized human brain organoids. *Nat Biotechnol* **36**:432–441. doi:10.1038/nbt.4127

Marton RM, Pașca SP. 2020. Organoid and Assembloid Technologies for Investigating Cellular Crosstalk in Human Brain Development and Disease. *Trends Cell Biol*. doi:10.1016/j.tcb.2019.11.004

Matsui TK, Tsuru Y, Hasegawa K, Kuwako K ichiro. 2021. Vascularization of human brain organoids. *Stem Cells* **39**:1017–1024. doi:10.1002/stem.3368

Medda X, Mertens L, Versweyveld S, Diels A, Barnham L, Bretteville A, Buist A, Verheyen A, Royaux I, Ebneth A, Cabrera-Socorro A. 2016. Development of a Scalable, High-Throughput-Compatible Assay to Detect Tau Aggregates Using iPSC-Derived Cortical Neurons Maintained in a Three-Dimensional Culture Format. *J Biomol Screen*. doi:10.1177/1087057116638029

Molyneaux BJ, Arlotta P, Menezes JRL, Macklis JD. 2007. Neuronal subtype specification in the cerebral cortex. *Nat Rev Neurosci* **8**:427–37. doi:10.1038/nrn2151

Nowakowski TJ, Bhaduri A, Pollen AA, Alvarado B, Mostajo-Radji MA, Di Lullo E, Haeussler M, Sandoval-Espinosa C, Liu SJ, Velmeshev D, Ounadjela JR, Shuga J, Wang X, Lim DA, West JA, Leyrat AA, Kent WJ, Kriegstein AR. 2017. Spatiotemporal gene expression trajectories reveal developmental hierarchies of the human cortex. *Science (80-)* **358**. doi:10.1126/science.aap8809

Nowakowski TJ, Pollen AA, Sandoval-Espinosa C, Kriegstein AR. 2016. Transformation of the Radial Glia Scaffold Demarcates Two Stages of Human Cerebral Cortex Development. *Neuron* **91**. doi:10.1016/j.neuron.2016.09.005

Pagliaro A, Finger R, Zoutendijk I, Bunschuh S, Clevers H, Hendriks D, Artegiani B. 2023. Temporal morphogen gradient-driven neural induction shapes single expanded neuroepithelium brain organoids with enhanced cortical identity. *Nat Commun* **14**. doi:10.1038/s41467-023-43141-1

Paşca AM, Sloan SA, Clarke LE, Tian Y, Makinson CD, Huber N, Kim CH, Park J-Y, O'Rourke NA, Nguyen KD, Smith SJ, Huguenard JR, Geschwind DH, Barres BA, Paşca SP. 2015. Functional cortical neurons and astrocytes from human pluripotent stem cells in 3D culture. *Nat Methods*. doi:10.1038/nmeth.3415

Paşca SP, Arlotta P, Bateup HS, Camp JG, Cappello S, Gage FH, Knoblich JA, Kriegstein AR, Lancaster MA, Ming G-L, Muotri AR, Park I-H, Reiner O, Song H, Studer L, Temple S, Testa G, Treutlein B, Vaccarino FM. 2022. A nomenclature consensus for nervous system organoids and assembloids. *Nat 2022 6097929* **609**:907–910. doi:10.1038/s41586-022-05219-6

Pellegrini L, Bonfio C, Chadwick J, Begum F, Skehel M, Lancaster MA. 2020. Human CNS barrier-forming organoids with cerebrospinal fluid production. *Science (80-)* **369**. doi:10.1126/science.aaz5626

Qian X, Nguyen HN, Song MM, Hadiono C, Ogden SC, Hammack C, Yao B, Hamersky GR, Jacob F, Zhong C, Yoon KJ, Jeang W, Lin L, Li Y, Thakor J, Berg DA, Zhang C, Kang E, Chickering M, Nauen D, Ho CY, Wen Z, Christian KM, Shi PY, Maher BJ, Wu H, Jin P, Tang H, Song H, Ming GL. 2016b. Brain-Region-Specific Organoids Using Mini-bioreactors for Modeling ZIKV Exposure. *Cell* **165**:1238–1254. doi:10.1016/j.cell.2016.04.032

Qian X, Su Y, Adam CD, Deutschmann AU, Pather SR, Goldberg EM, Su K, Li S, Lu L, Jacob F, Nguyen PTT, Huh S, Hoke A, Swinford-Jackson SE, Wen Z, Gu X, Pierce RC, Wu H, Briand LA, Chen HI, Wolf JA, Song H, Ming G. 2020. Sliced Human Cortical Organoids for Modeling Distinct Cortical Layer Formation. *Cell Stem Cell* **26**:766-781.e9. doi:10.1016/j.stem.2020.02.002

Qian Xuyu, Nguyen Ha Nam, Song MM, Hadiono C, Ogden Sarah C., Hammack Christy, Yao

Bing, Hamersky GR, Jacob F, Zhong C, Yoon K, Jeang W, Lin L, Li Yujing, Thakor J, Berg DA, Zhang Ce, Kang E, Chickering M, Nauen David, Ho C-Y, Wen Zhexing, Christian KM, Shi P-Y, Maher Brady J., Wu H, Jin P, Tang Hengli, Song H, Ming G, Bayer A, Lennemann NJ, Ouyang Y, Bramley JC, Morosky S, Marques ETJ, Cherry S, Sadovsky Y, Coyne CB, Ben-Ari Y, Spitzer NC, Blackshaw S, Scholpp S, Placzek M, Ingraham H, Simerly R, Shimogori T, Calvet G, Aguiar RS, Melo AS, Sampaio SA, Filippis I de, Fabri A, Araujo ES, Sequeira PC de, Mendonça MC de, Oliveira L de, al. et, Cauchemez S, Besnard M, Bompard P, Dub T, Guillemette-Artur P, Eyrolle-Guignot D, Salje H, Kerkhove MD Van, Abadie V, Garel C, al. et, Chung S, Hedlund E, Hwang M, Kim DW, Shin BS, Hwang DY, Kang UJ, Isacson O, Kim KS, Danjo T, Eiraku M, Muguruma K, Watanabe K, Kawada M, Yanagawa Y, Rubenstein JL, Sasai Y, Driggers RW, Ho CY, Korhonen EM, Kuivanen S, Jääskeläinen AJ, Smura T, Rosenberg A, Hill DA, DeBiasi RL, Vezina G, al. et, Faria NR, Azevedo RD, Kraemer MU, Souza R, Cunha MS, Hill SC, Thézé J, Bonsall MB, Bowden TA, Rissanen I, al. et, Garcez PP, Loiola EC, Costa RM da, Higa LM, Trindade P, Delvecchio R, Nascimento JM, Brindeiro R, Tanuri A, Rehen SK, Goodwin TJ, Schroeder WF, Wolf DA, Moyer MP, Haddow AD, Schuh AJ, Yasuda CY, Kasper MR, Heang V, Huy R, Guzman H, Tesh RB, Weaver SC, Hansen DV, Lui JH, Parker PR, Kriegstein AR, Heymann DL, Hodgson A, Sall AA, Freedman DO, Staples JE, Althabe F, Baruah K, Mahmud G, Kandun N, Vasconcelos PF, al. et, Jaffe AE, Shin J, Collado-Torres L, Leek JT, Tao R, Li C, Gao Y, Jia Y, Maher B.J., Hyde TM, al. et, Jessup JM, Goodwin TJ, Spaulding G, Kadoshima T, Sakaguchi H, Nakano T, Soen M, Ando S, Eiraku M, Sasai Y, Kim JY, Liu CY, Zhang F, Duan X, Wen Z., Song J, Feighery E, Lu B, Rujescu D, Clair DS, al. et, Kriks S, Shim JW, Piao J, Ganat YM, Wakeman DR, Xie Z, Carrillo-Reid L, Auyeung G, Antonacci C, Buch A, al. et, Kundakovic M, Gudsnuk K, Franks B, Madrid J, Miller RL, Perera FP,

Champagne FA, Lancaster MA, Knoblich JA, Lancaster MA, Renner M, Martin CA, Wenzel D, Bicknell LS, Hurles ME, Homfray T, Penninger JM, Jackson AP, Knoblich JA, Lazear HM, Govero J, Smith AM, Platt DJ, Fernandez E, Miner JJ, Diamond MS, Lui JH, Hansen DV, Kriegstein AR, Mariani J, Coppola G, Zhang P, Abyzov A, Provini L, Tomasini L, Amenduni M, Szekely A, Palejev D, Wilson M, al. et, Mlakar J, Korva M, Tul N, Popović M, Poljšak-Prijatelj M, Mraz J, Kolenc M, Rus KR, Vipotnik TV, Vodušek VF, al. et, Muguruma K, Nishiyama A, Kawakami H, Hashimoto K, Sasai Y, Paşca AM, Sloan SA, Clarke LE, Tian Y, Makinson CD, Huber N, Kim CH, Park JY, O'Rourke NA, Nguyen KD, al. et, Petanjek Z, Berger B, Esclapez M, Pollen AA, Nowakowski TJ, Chen J, Retallack H, Sandoval-Espinosa C, Nicholas CR, Shuga J, Liu SJ, Oldham MC, Diaz A, al. et, Roost MS, Iperen L van, Ariyurek Y, Buermans HP, Arindrarto W, Devalla HD, Passier R, Mummery CL, Carlotti F, Koning EJ de, al. et, Tang H., Hammack C., Ogden S.C., Wen Z., Qian X., Li Y., Yao B., Shin J, Zhang F, Lee EM, al. et, Thomsen ER, Mich JK, Yao Z, Hodge RD, Doyle AM, Jang S, Shehata SI, Nelson AM, Shapovalova NV, Levi BP, al. et, Wang W, Lufkin T, Wen Z., Nguyen H.N., Guo Z, Lalli MA, Wang X, Su Y, Kim NS, Yoon KJ, Shin J, Zhang C., al. et, Yin X, Mead BE, Safaee H, Langer R, Karp JM, Levy O, Yoon KJ, Nguyen H.N., Ursini G, Zhang F, Kim NS, Wen Z., Makri G, Nauen D., Shin JH, Park Y, al. et, Yu X, Zecevic N. 2016a. Brain-Region-Specific Organoids Using Mini-bioreactors for Modeling ZIKV Exposure. *Cell* **165**:1238–1254. doi:10.1016/j.cell.2016.04.032

Quadrato G, Nguyen T, Macosko EZ, Sherwood JL, Min Yang S, Berger DR, Maria N, Scholvin J, Goldman M, Kinney JP, Boyden ES, Lichtman JW, Williams ZM, McCarroll SA, Arlotta P. 2017. Cell diversity and network dynamics in photosensitive human brain organoids. *Nature* **545**:48–53. doi:10.1038/nature22047

Renner M, Lancaster MA, Bian S, Choi H, Ku T, Peer A, Chung K, Knoblich JA. 2017.

Self-organized developmental patterning and differentiation in cerebral organoids. *EMBO J* **36**:1316–1329. doi:10.15252/embj.201694700

Sarkar A, Mei A, Paquola ACM, Stern S, Bardy C, Klug JR, Kim S, Neshat N, Kim HJ, Ku M, Shokhirev MN, Adamowicz DH, Marchetto MC, Jappelli R, Erwin JA, Padmanabhan K, Shtrahman M, Jin X, Gage FH. 2018. Efficient Generation of CA3 Neurons from Human Pluripotent Stem Cells Enables Modeling of Hippocampal Connectivity In Vitro. *Cell Stem Cell* **22**:684-697.e9. doi:10.1016/j.stem.2018.04.009

Sawada T, Chater TE, Sasagawa Y, Yoshimura M, Fujimori-Tonou N, Tanaka K, Benjamin KJM, Paquola ACM, Erwin JA, Goda Y, Nikaido I, Kato T. 2020. Developmental excitation-inhibition imbalance underlying psychoses revealed by single-cell analyses of discordant twins-derived cerebral organoids. *Mol Psychiatry* **25**:2695–2711. doi:10.1038/s41380-020-0844-z

Shi Y, Kirwan P, Smith J, Robinson HPC, Livesey FJ. 2012. Human cerebral cortex development from pluripotent stem cells to functional excitatory synapses. *Nat Neurosci* **15**:477–86, S1. doi:10.1038/nn.3041

Tidball AM, Niu W, Ma Q, Takla TN, Walker JC, Margolis JL, Mojica-Perez SP, Sudyk R, Deng L, Moore SJ, Chopra R, Shakkottai VG, Murphy GG, Yuan Y, Isom LL, Li JZ, Parent JM. 2023. Deriving early single-rosette brain organoids from human pluripotent stem cells. *Stem Cell Reports* **18**:2498–2514. doi:10.1016/j.stemcr.2023.10.020

Uzquiano A, Kedaigle AJ, Pigoni M, Paulsen B, Adiconis X, Kim K, Faits T, Nagaraja S, Antón-Bolaños N, Gerhardinger C, Tucewicz A, Murray E, Jin X, Buenrostro J, Chen F, Velasco S, Regev A, Levin JZ, Arlotta P. 2022. Proper acquisition of cell class identity in organoids allows definition of fate specification programs of the human cerebral cortex. *Cell* **185**:3770-3788.e27. doi:10.1016/j.cell.2022.09.010

van Esbroeck ACM, Janssen APA, Cognetta AB, Ogasawara D, Shpak G, van der Kroeg M, Kantae V, Baggelaar MP, de Vrij FMS, Deng H, Allarà M, Fezza F, Lin Z, van der Wel T, Soethoudt M, Mock ED, den Dulk H, Baak IL, Florea BI, Hendriks G, De Petrocellis L, Overkleeft HS, Hankemeier T, De Zeeuw CI, Di Marzo V, Maccarrone M, Cravatt BF, Kushner SA, van der Stelt M. 2017. Activity-based protein profiling reveals off-target proteins of the FAAH inhibitor BIA 10-2474. *Science (80-)* **356**:1084–1087. doi:10.1126/science.aaf7497

Velasco S, Kedaigle AJ, Simmons SK, Nash A, Rocha M, Quadrato G, Paulsen B, Nguyen L, Adiconis X, Regev A, Levin JZ, Arlotta P. 2019. Individual brain organoids reproducibly form cell diversity of the human cerebral cortex. *Nature* 1. doi:10.1038/s41586-019-1289-x

Wang M, Gage FH, Schafer ST. 2023. Transplantation Strategies to Enhance Maturity and Cellular Complexity in Brain Organoids. *Biol Psychiatry* **93**:616–621. doi:10.1016/j.biopsych.2023.01.004

Xiang Y, Tanaka Y, Cakir B, Patterson B, Kim K-Y, Sun P, Kang Y-J, Zhong M, Liu X, Patra P, Lee S-H, Weissman SM, Park I-H. 2019. hESC-Derived Thalamic Organoids Form Reciprocal Projections When Fused with Cortical Organoids. *Cell Stem Cell* **24**:487-497.e7. doi:10.1016/J.STEM.2018.12.015

Yoon S-J, Elahi LS, Pașca AM, Marton RM, Gordon A, Revah O, Miura Y, Walczak EM, Holdgate GM, Fan HC, Huguenard JR, Geschwind DH, Pașca SP. 2019. Reliability of human cortical organoid generation. *Nat Methods* **16**:75–78. doi:10.1038/s41592-018-0255-0

Yuan SH, Martin J, Elia J, Flippin J, Paramban RI, Hefferan MP, Vidal JG, Mu Y, Killian RL, Israel MA, Emre N, Marsala S, Marsala M, Gage FH, Goldstein LSB, Carson CT. 2011.

Cell-Surface Marker Signatures for the Isolation of Neural Stem Cells, Glia and Neurons Derived from Human Pluripotent Stem Cells. *PLoS One* **6**:e17540. doi:10.1371/journal.pone.0017540

Zhang Y, Pak C, Han Y, Ahlenius H, Zhang Z, Chanda S, Marro S, Patzke C, Acuna C, Covy J, Xu W, Yang N, Danko T, Chen L, Wernig M, Südhof TCCC. 2013. Rapid Single-Step Induction of Functional Neurons from Human Pluripotent Stem Cells. *Neuron* **78**:785–798. doi:10.1016/j.neuron.2013.05.029

Zhang Z, Wang X, Park S, Song H, Ming GL. 2023. Development and Application of Brain Region–Specific Organoids for Investigating Psychiatric Disorders. *Biol Psychiatry* **93**:594–605. doi:10.1016/j.biopsych.2022.12.015

Figure Titles and Legends

Figure 1 Adherent cortical organoid model. A Schematic representation of the differentiation protocol. **B/C/D** Representative NPCs from three different iPSC lines with markers SOX2, Nestin and FOXG1 (scale bar B, 50 µm; C/D, 20 µm). **E** Representative time course showing self-organization during differentiation, starting with radial organization between day 28 and day 42, seeding density 1500 NPCs per well (green is Live-stain from Viability/Cytotoxicity kit; scale bars left to right 100 µm, 150 µm, 100 µm, 100 µm). **F** Full well showing radial organization at day 42 in culture were only a few dead cells are visible in red in the dense centre of the structure, seeding density 1500 NPCs per well (scale bar, 500 µm).

Figure 2 Adherent cortical organoids show an organized network of neuronal and astrocyte subtypes. A MAP2+ somas and dendrites alongside Tau+/MAP2- axons show segregation of dendritic and axonal compartments, with SOX2+ progenitors concentrated in the center of the organoid (Day 75, 200µm). **B** MAP2+ and NeuN+ cells indicate mature neurons (Day 72, 50 µm). **C** Deep-layer cortical marker CTIP2 and upper layer marker CUX1 show rudimentary segregation of cortical layers in expected inside-out pattern (Day 64, 50 µm). **D** A subset of the MAP2-positive neurons are GAD67+ (white arrows), indicating the presence of an interneuron population in the cortical organoids (Day 60, 50 µm). **E** Astrocyte markers GFAP and S100β show the general radial pattern of astrocyte outgrowth (Day 66, 500 µm). **F/G/H** GFAP staining reveals the morphologies of different astrocyte subtypes (white arrows), including fibrous astrocytes (**F**, Day 65, 100 µm), protoplasmic astrocytes (**G**,

Day 65, 50 µm) and interlaminar astrocytes (**H**, Day 65, 100 µm). **I** Co-localization of astrocyte marker GFAP and PAX6 marks radial glia (white arrows) (Day 65, 50 µm).

Figure 3 Adherent cortical organoids form oligodendrocyte lineage cells. A Adherent cortical organoids show OPCs as early as 44 days, indicated by OPC marker NG2 (Day 44, 20 µm). **B/C** The NG2+ OPCs are still present in the cortical organoids after 4 months (Day 119, B 50 µm, C 20 µm). **D** Young oligodendrocytes start to emerge after 4 months indicated by rudimentary MBP staining (Day 119 100 µm and 20 µm). **E/F** After 5 months, MBP-positive oligodendrocytes show more mature morphology and initial wrapping of NF200+ axons (Day 148; E, 50 µm and 20 µm, F 5 µm). **G/H/I** Oligodendrocyte distribution at day 161 where the MBP+ oligodendrocytes sit between axons bundles and co-localize with NF200+ axons. (G/H/I Day 161, G 500 µm, H 100µm, I 10 µm)

Figure 4 Adherent cortical organoids show synaptic connectivity and network bursts. A Synapsin staining shows synapse formation along MAP2+ dendrites (Day 70, 20 µm). **B** Co-localization of pre-synaptic marker Synapsin and post-synaptic marker PSD-95 (Day 205, 20 µm). **C** MAP2+ dendrites and soma are decorated with Synapsin+ synapses (Day 251, 100 µm) **D** Overview of entire well, showing alignment of Synapsin staining with MAP2 (Day 251, 500 µm)**. E** Sparse labeling of neurons with AAV9.CamKII.eGFP allows detailed imaging of glutamatergic dendritic spines with mature mushroom morphology, contacting pre-synaptic Synapsin puncta (Day 310, 5 µm). **F** Snapshot of radially organized neurons transduced with AAV1.Syn.GCaMP6s.WPRE.SV40 (Day 60, 100 µm). **G** Calcium events per minute from 36 cells from 7 recordings (each showing a cluster of neurons) from 2 different cortical

organoids at day 61. **H** Network bursts per minute from 37 cells from 6 recordings from 2 different cortical organoids. **I** Percentage of events that are part of network bursts indicates that the majority of cells are involved in network burst activity. **J** Representative calcium traces from 2 different clusters in which cells are showing individual activity as well as network bursts where multiple cells are active simultaneously.

Supplementary Figure 1 Reproducibility of Neural Progenitor Cells and Adherent Cortical Organoids. A NPCs are positive for SOX2, Nestin, FOXG1, PAX6 and TBR2 (scale bars 20 µm) **B** LIVE/DEAD staining of adherent organoids (N=4) showing reproducibility of the structure formation. Seeding density line 1; 1250 NPCs, line 2; 750 NPCs, line 3; 1000 NPCs (scale bars 500 µm). **C** Function of the necessary NPC seeding density to form adherent cortical organoids in relation to the doubling time as a measure of the proliferation rate of the NPCs. The doubling time of the NPCs explains more than half the variation (r^2 = 0.67) of the required seeding density showing that fewer cells need to be seeded for NPC lines with a higher proliferation rate. **D** Proportion of successful, single structure adherent cortical organoids. Each dot represents a different batch of adherent cortical organoids where the size of the batch ranges from 10-40 organoids.

Supplementary Figure 2 Neuronal maturation in cortical organoids is shown by a temporal shift in NPC and neuronal markers. A Representative images exhibiting change in expression of NPC and neuronal markers over time. Number of cells positive for NPC markers SOX2 and PAX6 decreases over time. Deep-layer CTIP2+ neurons start appearing at day 28, while upper-layer CUX1+ positive neurons appear in higher numbers around day 56.

(Scale bars 20 µm). **B** The percentages of DAPI+ cells expressing each of the markers were quantified at four time points. Significant differences between week 2 and week 8 expression were seen for SOX2+ (down by 39.6 %), CTIP2+ (up by 13.5 %) and CUX1+ cells (up by 23.1 %). *** $p < 0.0001$, ANOVA one-way followed by Tukey- Kramer's multiple correction test. Error bars indicate SEM, n=3-6 images taken over two wells, for each time point.

Supplementary Figure S3 Distribution of axons and dendrites in adherent cortical organoids Radially organized MAP2+/Tau+ dendrites along with both radially and circumferentially organized NF200+/Tau+ axons in duplicate for each cell line (Day 63, scale bars 500 µm)

Supplementary Figure S4 Cortical layering in the adherent cortical organoids A Rudimentary separation of SOX2+ NPCs, CTIP2+ deep layer neurons and CUX1+ upper layer neurons (Day 67, scale bar 100 µm) **B-E** Separation of CUX1 and CUX2 expression (B day 70, scale bar 100 µm; C day 70, scale bar 500 µm; D day 67, scale bar 500 µm; E day 67, scale bar 100 µm)

Supplementary Figure S5 GAD67+ interneurons make up a small proportion of NeuN+ neurons in the adherent cortical organoids A Example image of GAD67+ interneuron proportion of NeuN+ neurons (Day 67, 50 µm). **B** Quantification of GAD67+ proportion of NeuN+ neurons. Every point is the percentage of GAD67+ interneurons out of all NeuN+ neurons in a spatially randomized selected image with on average 130.6 (± 16.1) NeuN+

nuclei per frame. (Line 1: N= 26 images of 6 different cortical organoids at day 65-67; Line 2/3: 6 images of 2 different organoids at day 65).

Supplementary Figure S6 Astrocyte distribution within Adherent Cortical Organoids The abundantly present GFAP+ and S100B+ astrocytes have a comparable distribution with the MAP2+ neurons in the adherent cortical organoids. The astrocytes show radial patterns with many somas located in the centre as well as a large presence outside the centre (Day 63, scale bars 500 µm).

Figure 4 – Video 1

Video showing 10 minutes of calcium imaging of an adherent cortical organoid at Day 61 using the genetically encoded calcium indicator AAV1.Syn.GCaMP6s.WPRE.SV40 (rainbow filter indicates increasing calcium signal ranging from blue to red, speed increase indicated by time stamp in top left corner).

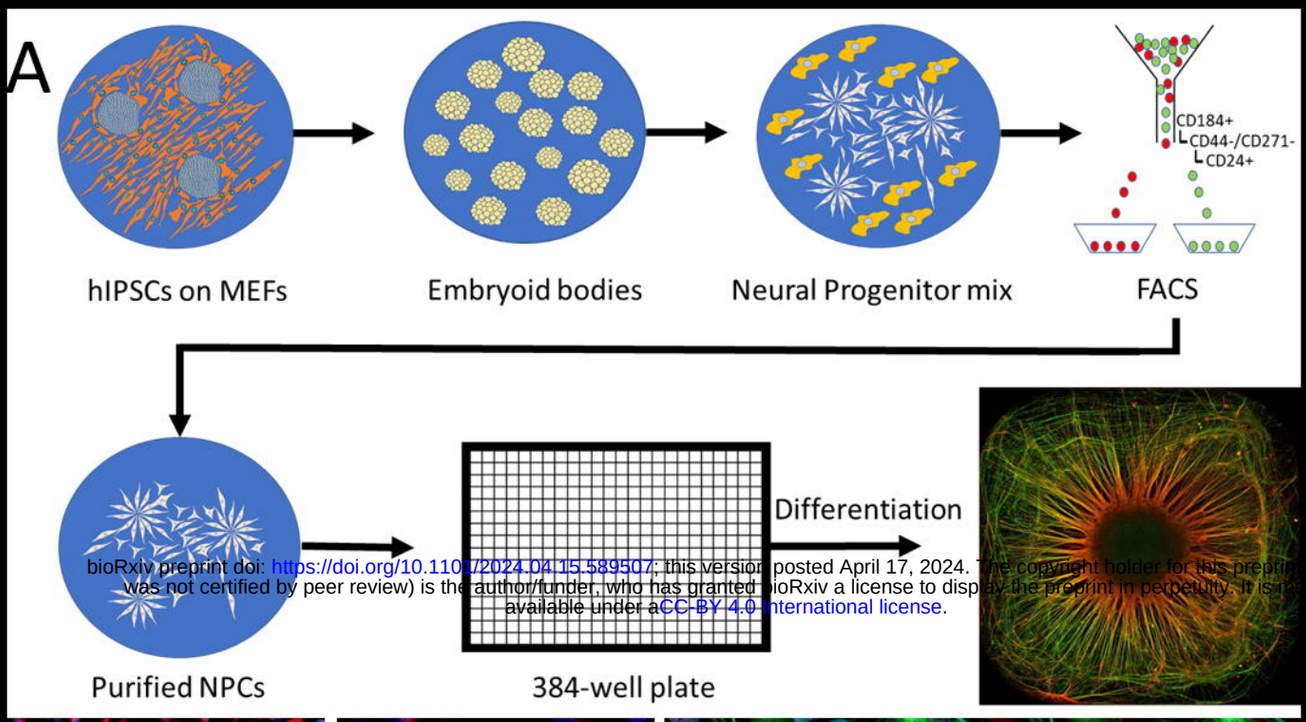

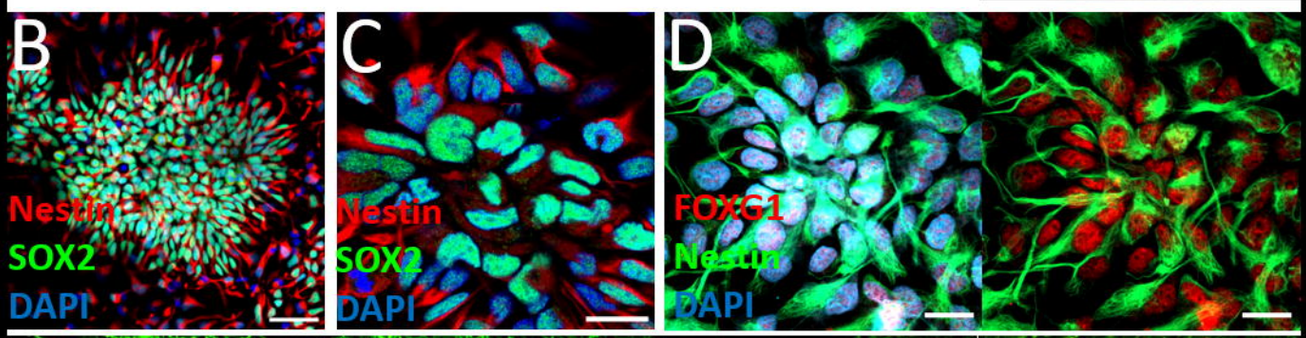

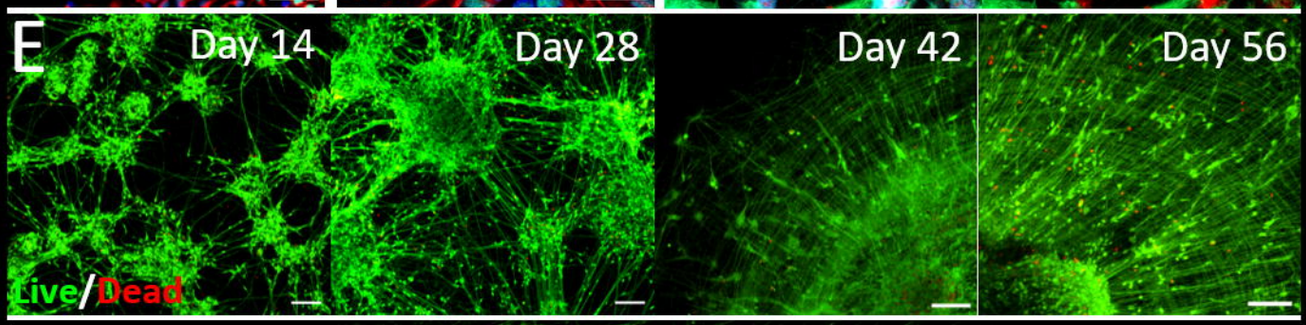

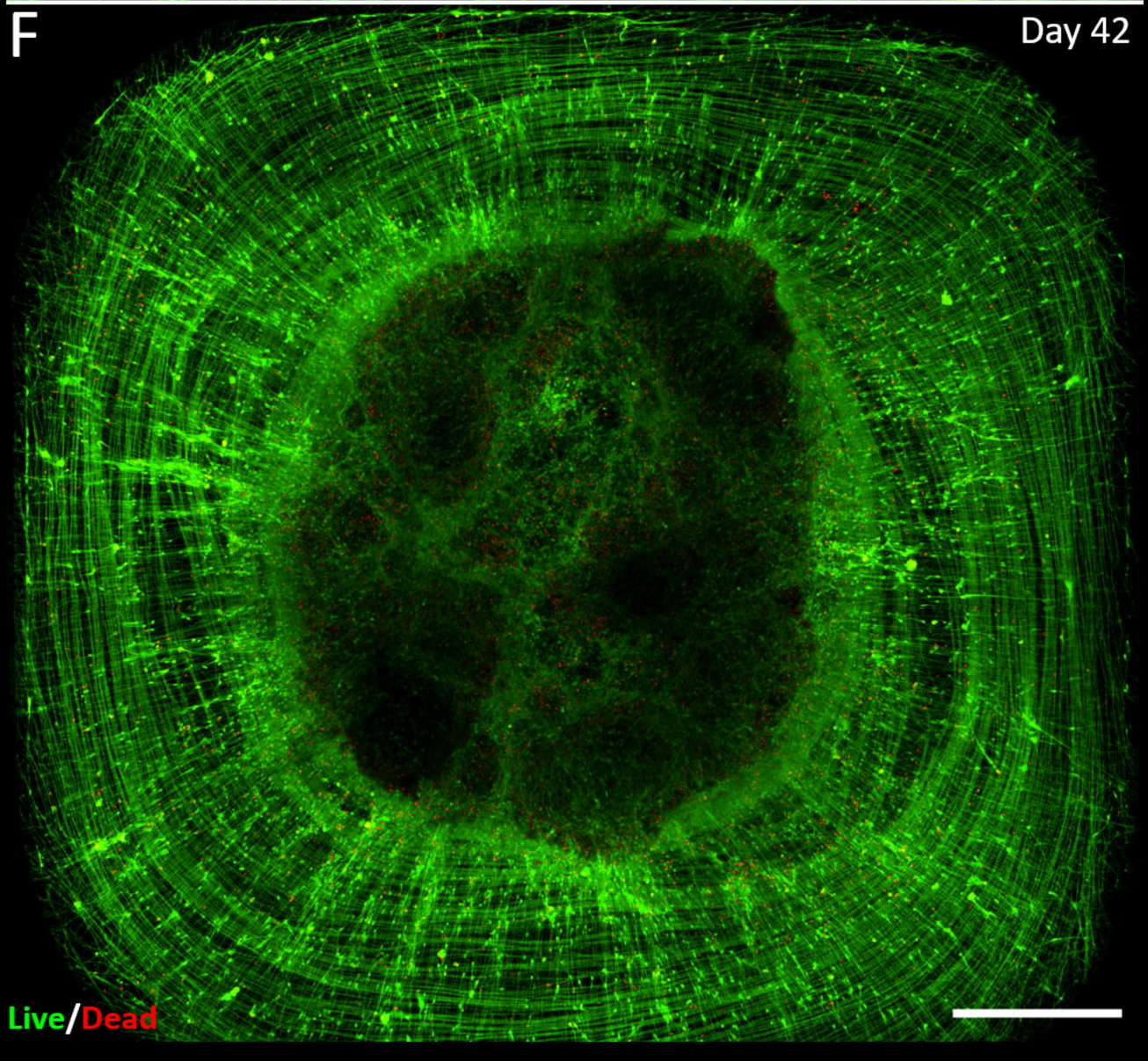

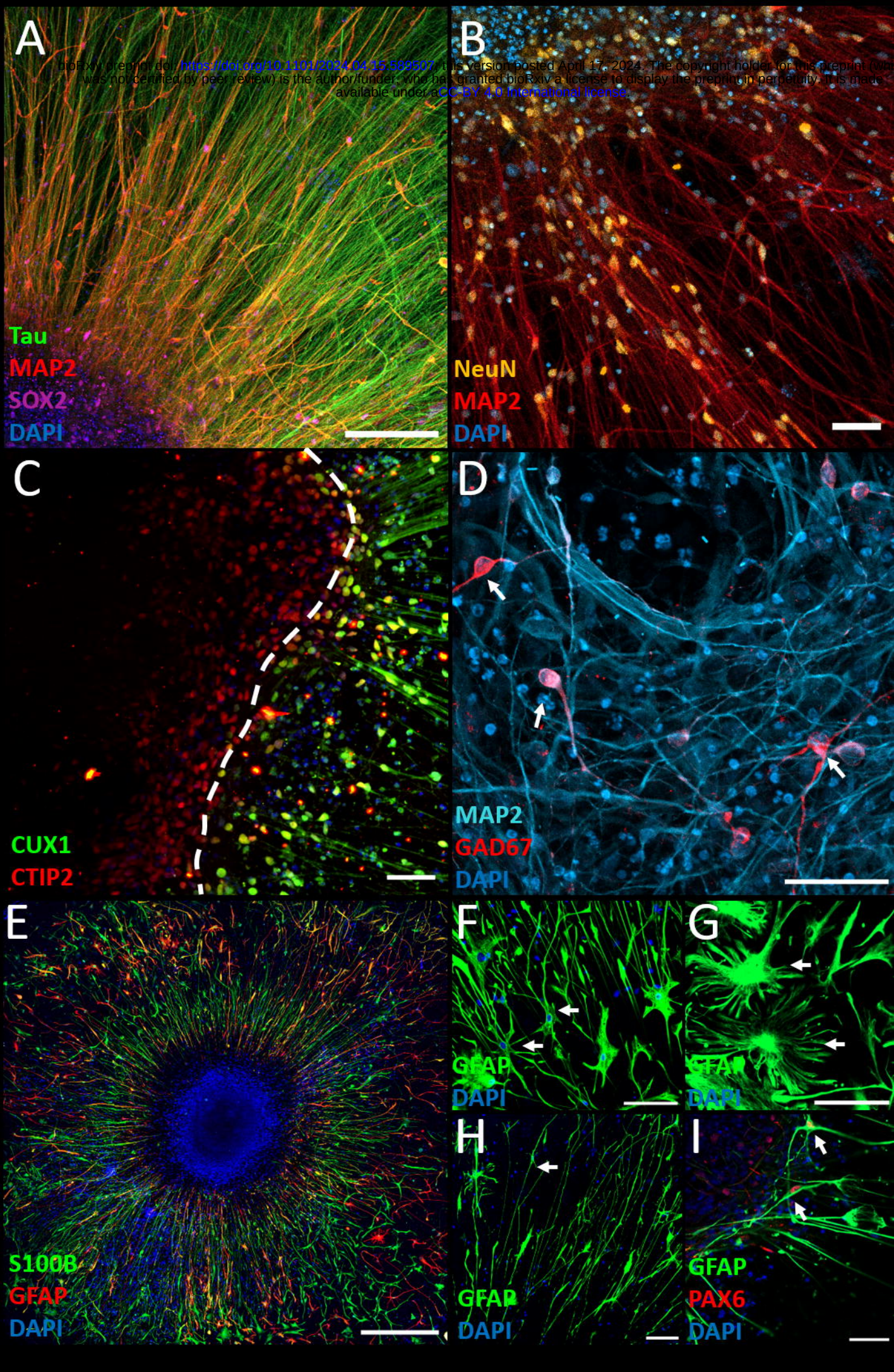

A Day 44
NG2
DAPI

B Day 119

C Day 119

D
NF200
MBP
MAP2
DAPI

Day 119

E
NF200
MBP
MAP2
DAPI

Day 148

F Day 148
NF200
MBP

G
NF200
MBP
MAP2
DAPI

Day 161

H Day 161
NF200
MBP
MAP2
DAPI

I Day 161
NF200
MBP
MAP2
DAPI

A
Day 70
Synapsin
MAP2
DAPI

B
Day 205
Synapsin
MAP2
PSD-95

C
Day 251
Synapsin
MAP2

D
Day 251
MAP2
Tau
DAPI
Synapsin

E
Day 310
Synapsin
CamKII.eGFP

F
Day 60
Syn.GCaMP6s

G
Events/min

H
NB/min

I
% events part of NB

J
Inferred calcium trace (ΔF/F)
Time (s)
Cluster 1
Cluster 2
Spike threshold
Spike
Network burst